
Article:
MacGregor-Chatwin, C., Jackson, P.J. orcid.org/0000-0001-9671-2472, Sener, M. et al. (9 more authors) (2019) Membrane organization of photosystem I complexes in the most abundant phototroph on Earth. Nature Plants, 5 (8). pp. 879-889. ISSN 2055-026X

https://doi.org/10.1038/s41477-019-0475-z

Membrane organisation of photosystem I complexes in the most abundant phototroph on Earth

C MacGregor-Chatwin[1], PJ Jackson[1,2], M Sener[3,4], JW Chidgey[1], A Hitchcock[1], P Qian[1], GE Mayneord[1], MP Johnson[1], Z Luthey-Schulten[3,4], MJ Dickman[2], DJ Scanlan[5] and CN Hunter[1]*

[1]Department of Molecular Biology and Biotechnology, University of Sheffield, Sheffield, UK.

[2]ChELSI Institute, ChELSI Institute, Department of Chemical and Biological Engineering, University of Sheffield, Sheffield, UK.

[3]Beckman Institute for Advanced Science and Technology, University of Illinois at Urbana-Champaign, Urbana, Illinois 61801.

[4]Department of Physics, University of Illinois at Urbana-Champaign, Urbana, Illinois 61801.

[5]Department of Biological Sciences, University of Warwick, Coventry CV4 7AL.

*email: c.n.hunter@sheffield.ac.uk

Abstract

Prochlorococcus is a major contributor to primary production, and it is the most globally abundant photosynthetic genus of picocyanobacteria because it can adapt to highly stratified low-nutrient conditions that are characteristic of the surface ocean. Here we examine the structural adaptations of the photosynthetic thylakoid membrane that enable different *Prochlorococcus* ecotypes to occupy high-light (HL), low-light (LL) and nutrient-poor ecological niches. We used atomic force microscopy (AFM) to image the different photosystem I (PSI) membrane architectures of the MED4 (HL) *Prochlorococcus* ecotype acclimated to high-light and low-light conditions in addition to the MIT9313 (LL) and SS120 (LL) *Prochlorococcus* ecotypes acclimated to low-light conditions. Mass spectrometry quantified the relative abundance of PSI, photosystem II (PSII) and cytochrome b_6f complexes and the various Pcb proteins in the thylakoid membrane. AFM topographs and structural modelling revealed a series of specialised PSI configurations, each adapted to the environmental niche occupied by a particular ecotype. MED4 PSI domains were loosely packed in the thylakoid membrane, whereas PSI in the LL MIT9313 is organised into a tightly-packed pseudo-hexagonal lattice that maximises harvesting and trapping of light. There are approximately equal levels of PSI and PSII in MED4 and MIT9313, but nearly two-fold more PSII than PSI in SS120, which also has a lower content of cytochrome b_6f complexes. SS120 has a different tactic to cope with low-light levels, and SS120 thylakoids contained hundreds of closely packed Pcb-PSI supercomplexes that economise on the extra iron and nitrogen required to assemble PSI-only domains. Thus, the abundance and widespread distribution of *Prochlorococcus* reflect the strategies that various ecotypes employ for adapting to limitations in light and nutrient levels.

Introduction

By virtue of its abundance in the oceans *Prochlorococcus* is one of the most important photosynthetic organisms on Earth. A global abundance of 2.9 ± 0.1 x 10^{27} *Prochlorococcus* cells fixes 4 gigatonnes of carbon per year[1], which is comparable to the total primary productivity of the world's croplands[2]. *Prochlorococcus* is found in the oligotrophic ocean with a distribution between approximately 45 °N and 40 °S and is present throughout the euphotic zone down to a depth of about 200 metres[3]. *Prochlorococcus* is also notable for its unique pigmentation, being the only type of marine phytoplankton to use divinyl derivatives of chlorophyll *a* and *b* (Chl *a* and Chl *b*), bound to Pcb proteins, to capture light energy and drive photosynthesis[4]. *Prochlorococcus* chlorophylls exceed 50% of marine chlorophyll mass in large expanses of the ocean[3,5].

There are seven major clades of *Prochlorococcus* and evolutionary diversification has been strongly tied to environmental conditions with clades broadly classified as being either high light (HL)-adapted or low light (LL)-adapted ecotypes[6-12]. HL-adapted ecotypes such as MED4 and MIT9312 have a lower Chl *b*:Chl *a* ratio, and are typically the most abundant organisms in oligotrophic surface waters of the open ocean although they are present throughout the entire euphotic zone[13-16]. LL-adapted ecotypes such as NATL2A, SS120 and MIT9313 have a higher Chl *b*:Chl *a* ratio and grow optimally under much lower light intensities[8,17]. Elevated Chl *b* levels allow these strains to absorb more light in the blue region of the spectrum, which is prevalent at the lower depths in the euphotic zone[18], conferring a competitive advantage in this ecological niche[17].

Prochlorococcus differs from marine *Synechococcus*, with which it shares a relatively recent common ancestor[10,12,19-21], in that its light-harvesting antenna complexes are formed from integral membrane Pcb proteins, rather than the membrane-extrinsic phycobilisome complexes found in most cyanobacteria[22]. Pcb proteins have six transmembrane helices, and significant homology with the chlorophyll binding PSII subunit CP43 and the iron-limitation IsiA[23,24] protein. *Prochlorococcus* ecotypes rely on different Pcb-PSI supercomplexes to meet their light harvesting requirements; in SS120 light-harvesting capacity is enhanced by surrounding PSI trimers with an 18-membered PcbG ring ($PcbG_{18}PSI_3$)[25,26], similar to the IsiA-PSI supercomplex found in *Synechocystis* when grown under iron limited conditions[27,28]. In SS120 and MIT9313 PSII dimers are flanked by 8 Pcb proteins (Pcb_8PSII_2)[24,26]. The HL-adapted ecotype MED4 does not produce an 18 membered Pcb-PSI supercomplex in iron rich or depleted conditions, although it does appear to assemble a Pcb-PSII supercomplex[26].

Taking into account the abundance of *Prochlorococcus* in the oceans, with each cell housing roughly 5 μm^2 of thylakoids[29], we estimate that the combined surface area of energy-absorbing *Prochlorococcus* membranes is 28 times the surface area of the Earth. Despite the global importance and scale of these membranes, little is known about their supramolecular organisation and how they vary between different ecotypes to allow adaptation to different light and nutrient conditions. Photosynthetic membrane organisation can be probed by atomic force microscopy (AFM)[30-38]. AFM of cyanobacterial thylakoids from *Thermosynechococcus elongatus* and *Synechococcus* sp. PCC 7002 revealed long-range semi-crystalline PSI-only membrane arrays, and more heterogeneous membrane domains where PSI is interspersed amongst membrane complexes such as PSII and the cytochrome b_6f complex[39]. AFM of thylakoid membranes from *Synechococcus* sp. PCC 7942 showed a disordered membrane system with PSI intermixed with PSII, which was co-localised with the cytochrome b_6f

complex[40]. Here, we use a combination of AFM, mass spectrometry and pigment analysis to elucidate the organisation and composition of photosynthetic membranes from *Prochlorococcus*, to see how membrane architectures vary with ecotype and how they are optimised to function in their respective ecological niches in order to harvest, transfer and trap light energy.

Results

Supramolecular organisation of thylakoids from the high light-adapted MED4 ecotype grown under low-light

Purified thylakoid membranes were prepared from cells of the MED4 ecotype grown at 5 µmol photons m^{-2} s^{-1}, by fractionation on continuous sucrose gradients containing 0.1% digitonin (Supplementary Fig. 1). AFM analysis of membrane samples collected from throughout the sucrose gradient showed multiple membrane patches housing trimeric protein complexes (Fig. 1a,b,d,e), which were reminiscent of the PSI complexes in AFM topographs of *T. elongatus* thylakoids[39]. As no crystal structure of the MED4 PSI complex is available, the structure of the *T. elongatus* PSI trimer (PDB ID: 1JB0) was used for reference (Fig. 1c). The trimeric features in the topographs had an average height above the mica surface and the lipid bilayer of 10.1 ± 0.6 nm and 3.4 ± 0.3 nm respectively; the average lateral distance between monomers was 10.4 ± 0.9 nm. These dimensions are consistent with the trimeric PSI structure[41-43] and were assigned as such.

The somewhat disorganised arrangement of trimeric PSI complexes in MED4 membrane patches (Fig. 1a,b) differs from the paracrystalline PSI organisation often found in AFM topographs of *T. elongatus* membranes[39]. However, for both paracrystalline and disorganised PSI domains, the high density of PSI packing appears to preclude the presence of other protein complexes, and there was no evidence in AFM topographs for PSII, cytochrome b_6f complex or Pcb antenna complexes in these MED4 membranes. The density of PSI complexes was calculated for the membrane patches shown in Fig. 1a; for ease of comparison, the data were calculated as PSI monomer equivalents rather than whole trimers. The membrane densities were 4604 (left) and 5203 (right) PSI monomer equivalents per μm^2 and for the membrane patch in Fig. 1b it was calculated to be 3102 complexes per μm^2. Using a value of 96 chlorophyll molecules per PSI monomer the density of chlorophyll in these membrane patches was calculated as 442024, 499510 and 293236 molecules of chlorophyll per μm^2 of thylakoid membrane respectively.

Another feature of the MED4 membrane patches was the presence of dimeric and monomeric complexes (highlighted by dotted ovals and a white asterisk in Fig. 1e respectively); these complexes have been assigned as dimeric and monomeric PSI on the basis of their height and their lateral dimensions. This is consistent with membrane patches from *T. elongatus*[39] where several membrane patches were imaged that contained monomeric, dimeric and trimeric PSI complexes. The combined ratio of PSI monomer equivalents in trimeric vs monomeric or dimeric PSI in the membrane patches in Fig 1a is 5.3.

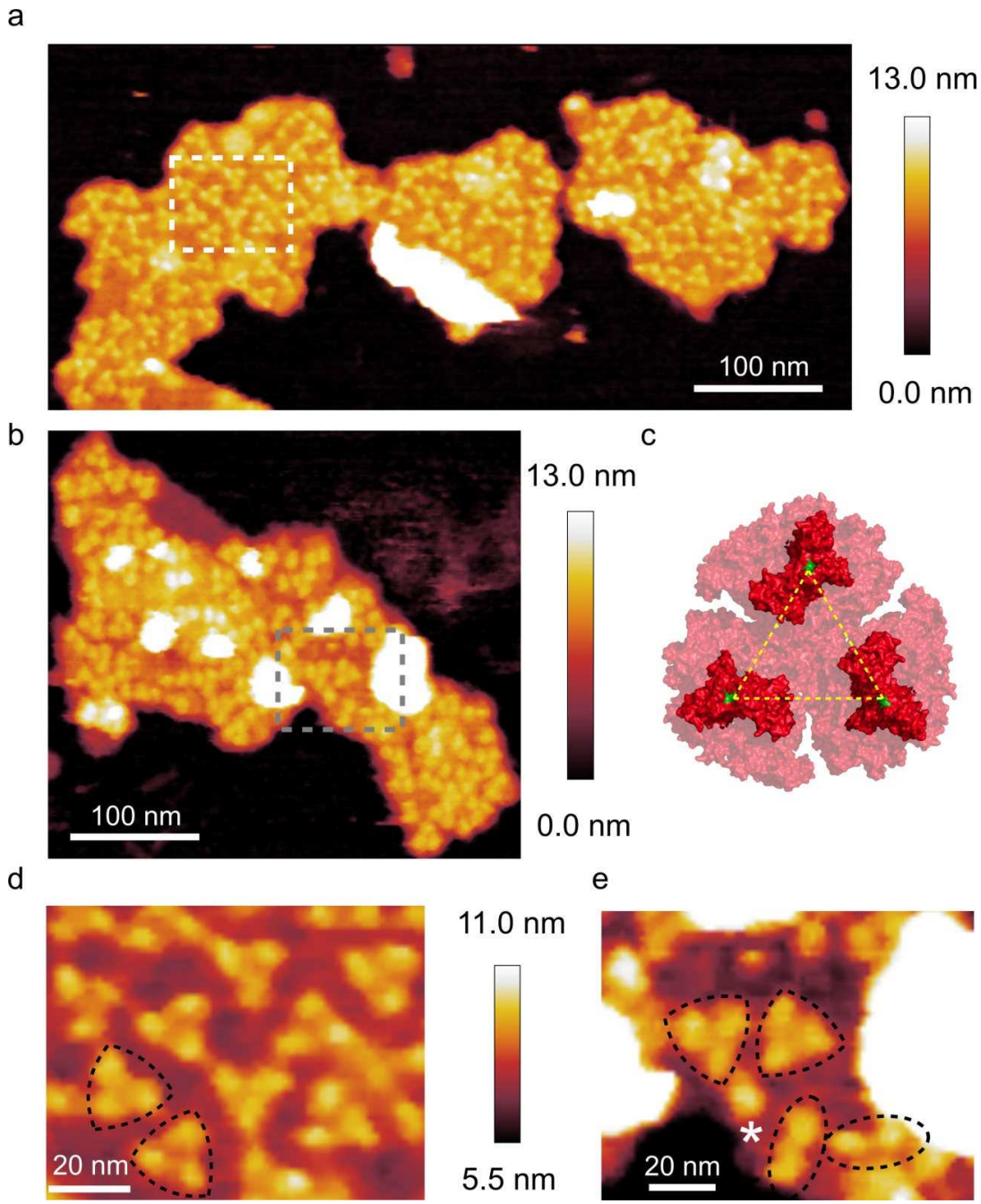

Fig. 1 AFM of PSI in thylakoid membrane patches from low-light grown MED4. (a) AFM topograph of a membrane patch showing trimeric PSI complexes; the area delineated by the white box is shown in (d). (b) A second membrane patch also showing PSI, which has a more disorganised, less densely packed architecture; the area delineated by the grey box is shown in (e). (c) The crystal structure of the trimeric PSI complex from *T. elongatus* seen from the cytoplasmic face of the membrane (PDB ID: 1JB0). The yellow lines represent a distance of 9.1 nm measured from proline 29 (green) of the PsaC subunit. (d) Zoomed view of the area highlighted in (a) showing the trimeric PSI complexes (outlined in black) in more detail. (e) Zoomed view of the area outlined in (b). Trimeric, dimeric and monomeric PSI complexes are highlighted with black triangles, black ovals and white asterisks respectively.

Supramolecular organisation of thylakoids from the HL-adapted MED4 ecotype grown under high-light

In thylakoid membranes purified from MED4 cells grown in high light the PSI complexes have a disordered distribution similar to that of the thylakoid membranes purified from low-light cells. The density of PSI complexes in these high light membrane patches is generally lower that their low-light counterparts and is highly variable; the PSI densities of membrane patches in Fig. 2a-c are 4283, 3742 and 2635 PSI monomer equivalents per μm^2 of thylakoid membrane, respectively. Using a value of 96 chlorophyll molecules per PSI monomer equivalent the chlorophyll density of these patches was calculated at 411168, 359232 and 252960 chlorophyll molecules per μm^2 of thylakoid membrane, respectively, somewhat lower than for low light MED4 (442024, 499510 and 293236 chlorophyll molecules per μm^2). Another difference between high-light and low-light membranes is the proportion of PSI complexes in a trimeric configuration; the combined number of PSI complexes (as monomer equivalents) forming trimers in the high light membrane patches from Fig. 2a-c is 132. There are also proportionally more PSI complexes in either a dimeric or monomeric state; the combined total (monomers plus dimers) from the three membrane patches in Fig. 2 is 121 giving a ratio of trimeric to non-trimeric PSI complexes of 1.09, significantly lower than the 5.3 observed for low light adapted membranes. In summary, the effect of increasing the light used to grow MED4 from 5 to 250 µmol photons m^{-2} s^{-1}, is a reduced packing density of PSI complexes, lower by approximately 17% on average, and a significantly reduced population of PSI trimers, in favour of more monomers and dimers.

.

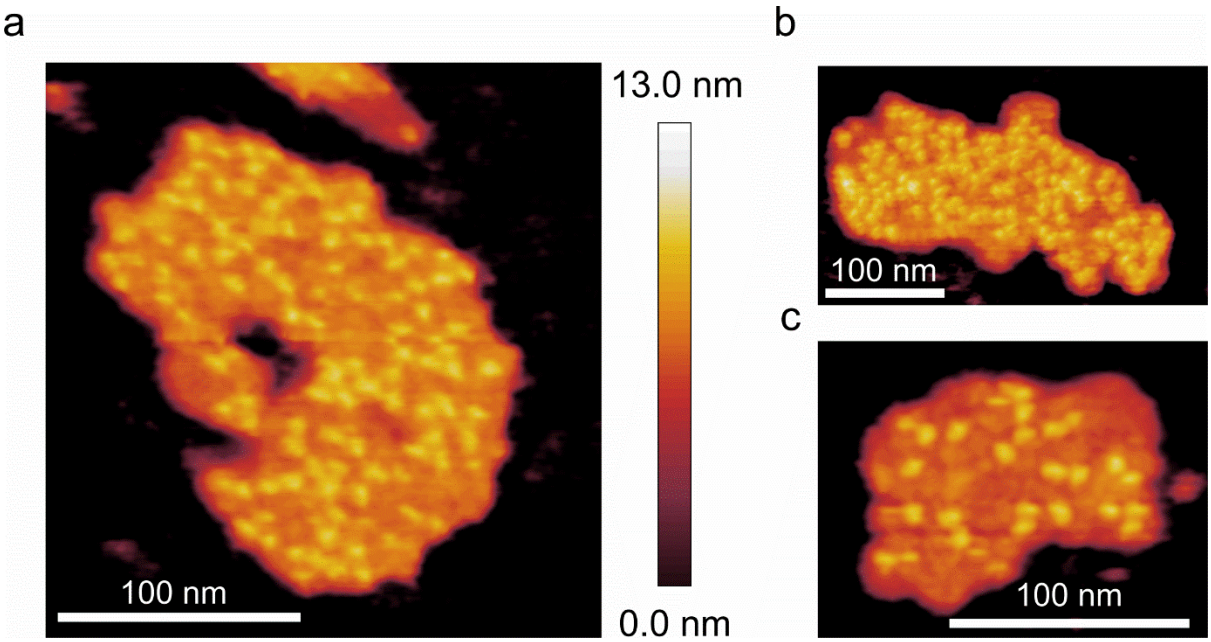

Fig. 2 AFM of PSI in high-light adapted MED4 thylakoid membrane patches. (a) and (b) AFM topographs of membrane patches showing PSI complexes at a relatively high density. (c) AFM topograph of a membrane patch with a lower density of PSI complexes.**AFM of thylakoid membranes from the LL-adapted MIT9313 ecotype**

155 Trimeric PSI complexes could also be imaged in thylakoid membranes from MIT9313 cells, but their
156 organisation differed from that seen in MED4 membrane patches. Fig. 2a-d shows that MIT9313 PSI
157 complexes were almost exclusively organised into a pseudo-hexagonal lattice (Fig. 2d), similar to the
158 paracrystalline PSI-only domains of thylakoid membranes from *T. elongatus*[39], an arrangement that
159 leaves no room for PSII, cytochrome b_6f complex or Pcb antenna proteins. In this LL-adapted ecotype,
160 the tight packing of PSI complexes increases the abundance of PSI in the thylakoid membrane relative
161 to the HL-adapted MED4 ecotype, with 5377, 5982 and 5391 PSI complexes per μm^2 and 516258,
162 574302 and 517572 molecules of chlorophyll per μm^2 in Fig. 2a-c respectively. Unlike MED4, PSI
163 complexes in the MIT9313 membranes are nearly all trimeric, with few PSI monomers and dimers; the
164 combined ratio of trimeric to non-trimeric PSI (that is, PSI monomers and dimers) in the patches in Fig
165 3 is 44.48, significantly higher than MED4 membrane patches grown under either high or low light.
166 The average height of the PSI complexes in the MIT9313 membrane patches from the mica and bilayer
167 surface is 10.1 ± 0.4 nm and 3.3 ± 0.4 nm respectively. The average distance between constituent
168 monomers of the trimeric PSI complexes from the MIT9313 membrane patches was 10.2 ± 0.7 nm.
169 These measurements are consistent with the crystal structure of the *T. elongatus* PSI trimer and
170 almost identical to the dimensions measured for the MED4 PSI trimer.

171

172

173

174

175

176

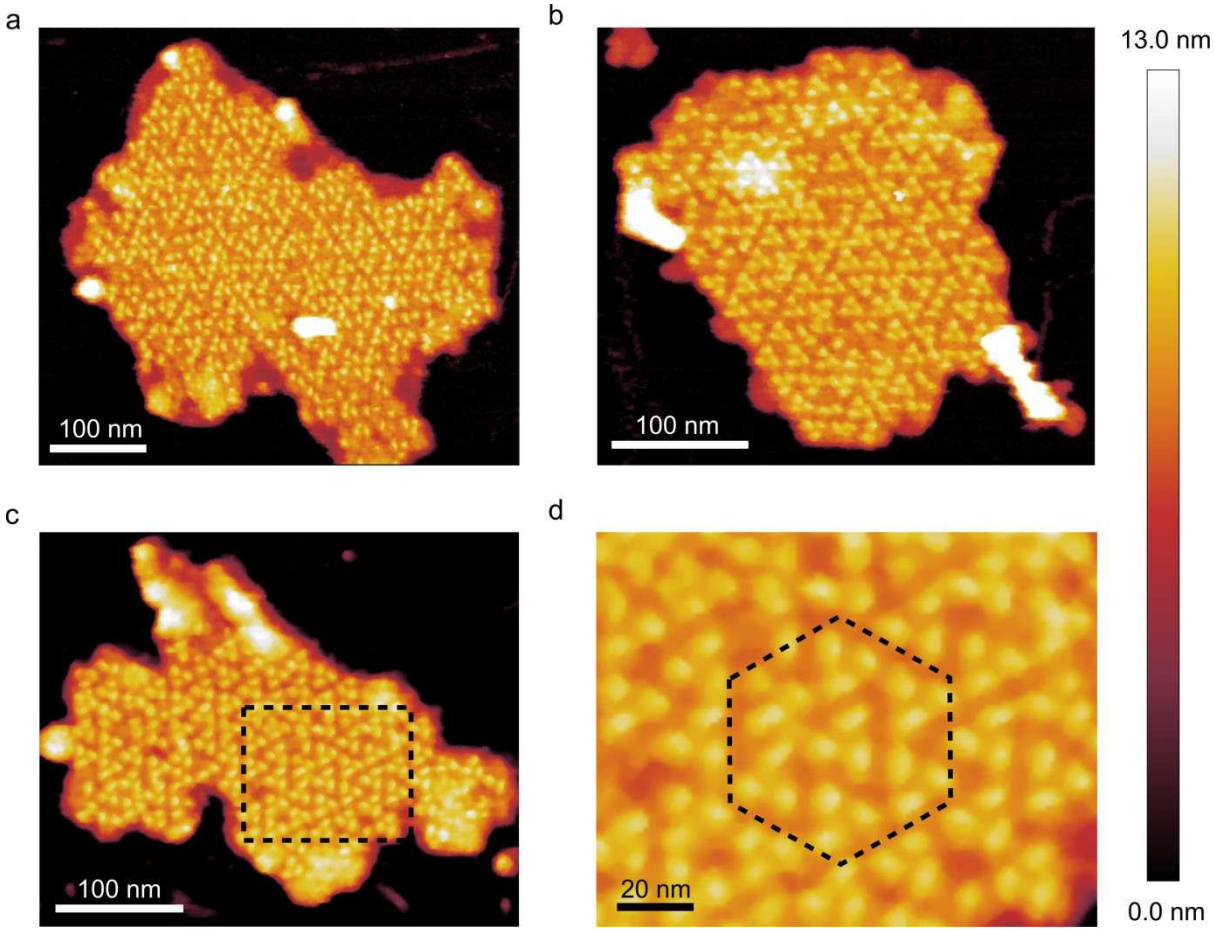

Fig. 3 AFM of PSI in thylakoid membrane patches from MIT9313. (a), (b) and (c) form a gallery of thylakoid membrane patches in which PSI is packed into a pseudo-hexagonal organisation; these large patches of PSI trimers do not appear to contain any other protein complexes. (d) Zoomed in view of the area highlighted in (c) with the "unit cell" of the hexagonally packed complexes outlined by the black dotted line.

AFM of thylakoid membranes from the LL-adapted SS120 ecotype

Solubilisation of membranes from the SS120 ecotype yields PSI supercomplexes, in which a PSI trimer is surrounded by an 18 membered ring of the Pcb protein[25,26]. However, the supramolecular arrangement of these Pcb-PSI supercomplexes was unknown, so AFM topographs were recorded for thylakoid membranes from SS120 (Fig. 3a,b), revealing several closely packed Pcb-PSI supercomplexes. The resolution is sufficient to identify individual components, including trimeric PSI cores, and each surrounding ring comprised of Pcb proteins (Fig. 3c,d). For comparison, a homologous PSI supercomplex, the IsiA-PSI supercomplex, was purified from an iron-limited *Synechocystis* sp. PCC 6803 culture and imaged by negative stain TEM. The projection map for the IsiA-PSI supercomplex (Fig. 3e), generated by averaging 52 particles, shows a trimeric PSI core surrounded by an 18-membered ring of the IsiA protein, a homologue of the PSII subunit CP43 and the light harvesting

antenna Pcb proteins. Fig. 3f shows a model of the IsiA-PSI supercomplex constructed from the PSI crystal structure (PDB ID:1JB0) and the CP43 subunit from the PSII crystal structure (PDB ID: 3WU2)[44], which shows the similarities between the Pcb-PSI supercomplexes in the AFM topographs and the IsiA-PSI structures. Furthermore, the average diameter of the putative Pcb ring in the AFM topographs was 32.8 ± 0.9 nm, consistent with the 33.0 nm diameter of the 18 membered Pcb ring determined by negative stain TEM of the isolated Pcb-PSI supercomplex[25].

It was also possible to image a much larger membrane patch that contained over a hundred Pcb-PSI supercomplexes (Fig. 4a). The average height of the PSI complexes in this membrane patch was 9.6 ± 0.2 nm above the mica surface and 3.4 ± 0.2 nm above the membrane bilayer, comparable to the height of the PSI crystal structure from *T. elongatus.*

The thylakoid membrane in Fig. 4 is very densely packed with Pcb-PSI supercomplexes (Fig. 4b,c), leaving no room for the other photosynthetic protein complexes such as PSII and the cytochrome b_6f complex, and indicating that "PSI-only" zones are a feature of all three ecotypes. The density of Pcb-PSI supercomplexes in the membrane patch shown in Fig. 4a is 893 per μm^2, equivalent to 2679 PSI complexes per μm^2. The average PSI density was 5583 PSI complexes per μm^2 for the other LL-adapted strain MIT9313; thus, the Pcb ring reduces the number of PSI complexes that can pack into the same area (Fig. 4d,e) and increases the distance between adjacent PSI trimers (Fig. 4f-h). The exact number of chlorophyll pigments bound to each type of Pcb protein is unavailable; however by sequence comparison with the IsiA protein from *Synechocystis* it is apparent that the two proteins are almost identical[24]. Assuming that each Pcb protein binds 15 chlorophyll molecules, the same number as the IsiA protein, the number of chlorophyll molecules in the Pcb-PSI supercomplex is 558[25]. Using this number the density of chlorophyll was calculated at 498294 molecules of chlorophyll per μm^2 based on the AFM data in Fig. 4. This density of chlorophyll molecules is comparable to the HL-adapted MED4 ecotype but not as high as the other LL-adapted ecotype MIT9313.

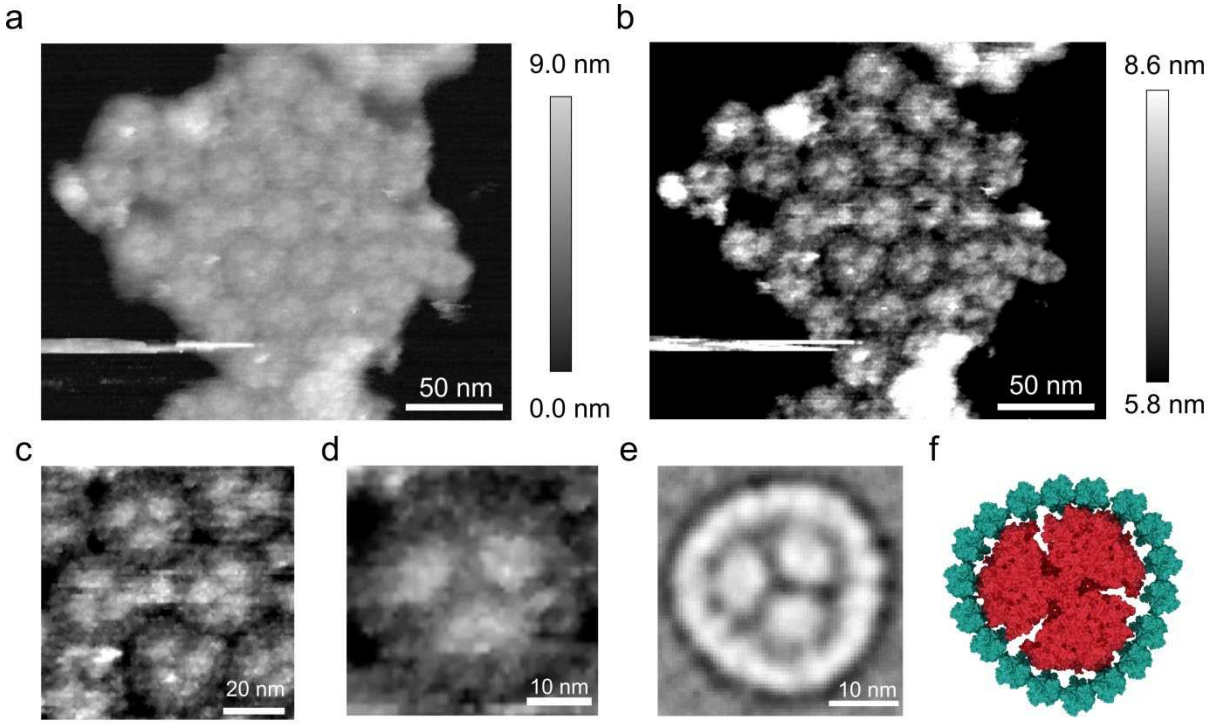

Fig. 4 AFM imaging of clustered Pcb-PSI supercomplexes in thylakoid membrane patches from SS120. (a) A cluster of approximately 30 closely packed Pcb-PSI supercomplexes (b) The same membrane patch as displayed in (a) with the z-scale altered to highlight the structural elements of the Pcb-PSI supercomplex. The trimeric PSI core can clearly be seen in several of the supercomplexes with individual Pcb subunits also visible in the rings surrounding the PSI trimer. (c) Zoomed in view of (b) showing the interactions between adjacent Pcb-PSI supercomplexes in the membrane patch in (a) and (b). (d) Zoomed view of the membrane patch in (a) and (b) showing a single Pcb-PSI supercomplex; the trimeric core can be clearly identified, as can subunits within the Pcb ring. (e) Averaged projection map of the top-down view of the IsiA-PSI supercomplex purified from iron-limited *Synechocystis* sp. PCC 6803, homologous structure to the Pcb-PSI supercomplex, and generated by averaging projections of 52 negatively stained particles taken at room temperature by transmission electron microscopy (TEM). This averaged projection map shows the trimeric PSI complexes surrounded by an 18 membered ring of the IsiA protein, a homologue of the Pcb and CP43 proteins. (f) Model of the Pcb-PSI supercomplex based on the AFM data in (b), the PSI crystal structure (PDB ID: 1JB0) and the crystal structure of the CP43 subunit from the PSII crystal structure (PDB ID: 3WU2).

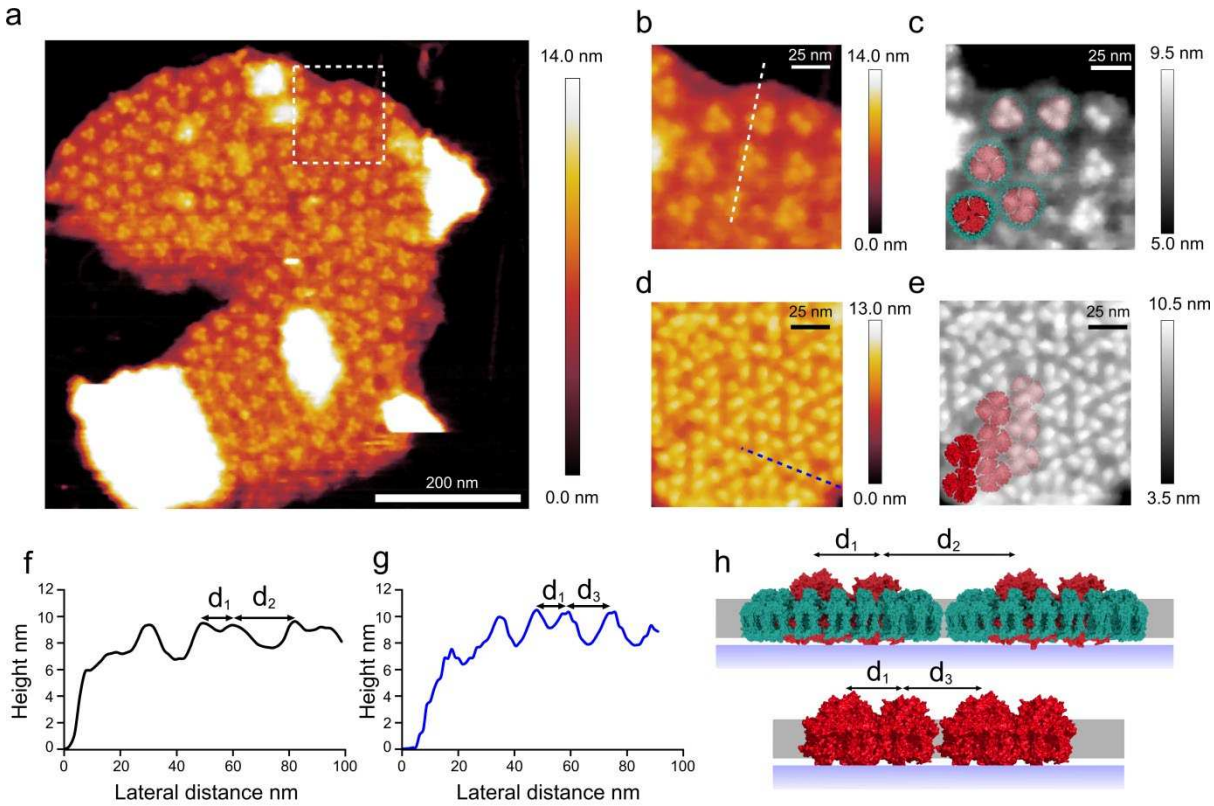

Fig. 5 Medium resolution AFM topograph of a large membrane patch from the SS120 ecotype (a) This image shows a membrane patch where the trimeric PSI core can be seen within hundreds of Pcb-PSI supercomplexes. (b) Magnified view of the area outlined by the white box in (a) showing the Pcb-PSI supercomplexes in more detail; the white line shows the location of the height profile in (f). (c) Grey scale of the same view as in (b) with the Pcb-PSI supercomplex model fitted to the AFM data. (d) An area of membrane from the MIT9313 membrane patch shown in Fig. 3c highlighting the difference in PSI packing between Pcb-PSI supercomplexes and "naked" PSI trimers in the thylakoid membrane; the presence of the Pcb ring in (b) leads to fewer PSI complexes per μm^2 of thylakoid membrane. The blue line shows the location of the height profile in (g). (e) Grey scale of the same area as (d) with the PSI crystal structure fitted to the AFM data. (f) Height profile of dashed white line in (b) showing distances between the PSI complexes; the distance between PSI monomers in the same supercomplex (d_1) is 9.3 nm and the distance between PSI monomers in adjacent supercomplexes (d_2) is 20.4 nm. (g) Height profile of dashed blue line in (d) showing distances between PSI complexes in "naked" PSI trimers; the distance between constituent monomers in the PSI trimer (d_1) is 10.1 nm, consistent with d_1 measured in Pcb-PSI supercomplexes. The distance between PSI monomers in adjacent PSI trimers (d_3) is measured at 14.0 nm, less than that measured from the Pcb-PSI supercomplexes owing to the absence of the Pcb ring. (h) A membrane model showing the distances between Pcb-PSI supercomplexes (top) and "naked" PSI trimers (bottom) with the distances measured from (f) and (g) shown.

Comparison of long range order of PSI complexes between *Prochlorococcus* ecotypes, MIT9313, MED4, SS120, and *T. elongatus*

Structural models based on AFM topographs were constructed for the PSI trimer containing thylakoid domains of *Prochlorococcus* ecotypes, MIT9313 (Figs. 2b, 5a), MED4 (Figs. 1a, 5b), SS120 (Figs. 4a, 5c, 5d), and compared to a corresponding *T. elongatus* membrane model[39] (Figs. 5e, 5f). The structural models reveal the packing pattern of constituent proteins, particularly the relative position and orientation of neighbouring PSI trimers, thereby permitting a comparison between the membrane architectures of different ecotypes (Fig. 5e). A near-periodic arrangement of PSI trimers, reported earlier for *T. elongatus* thylakoid domains[39], is observed for the MIT9313 ecotype (Fig. 2b, 5a, 5e); a strong orientational correlation between neighbouring PSI trimers is also present for MIT9313, but up to an arbitrary $\pi/3$ rotation of the trimers (Fig. 5f).

The packing patterns of MIT9313 and *T. elongatus* PSI domains are nearly identical (Fig. 5e), thereby implying that MIT9313 has similar inter-PSI exciton sharing properties as *T. elongatus*[39]. The model for the MED4 ecotype (Figs. 5b) represents a packing density of PSI trimers similar to that of MIT9313, but without any apparent periodicity (Fig. 5e). The presence of the surrounding Pcb units for SS120 (Fig. 5c) results in an increased trimer-trimer separation as well as a lack of periodicity (Fig. 5e).

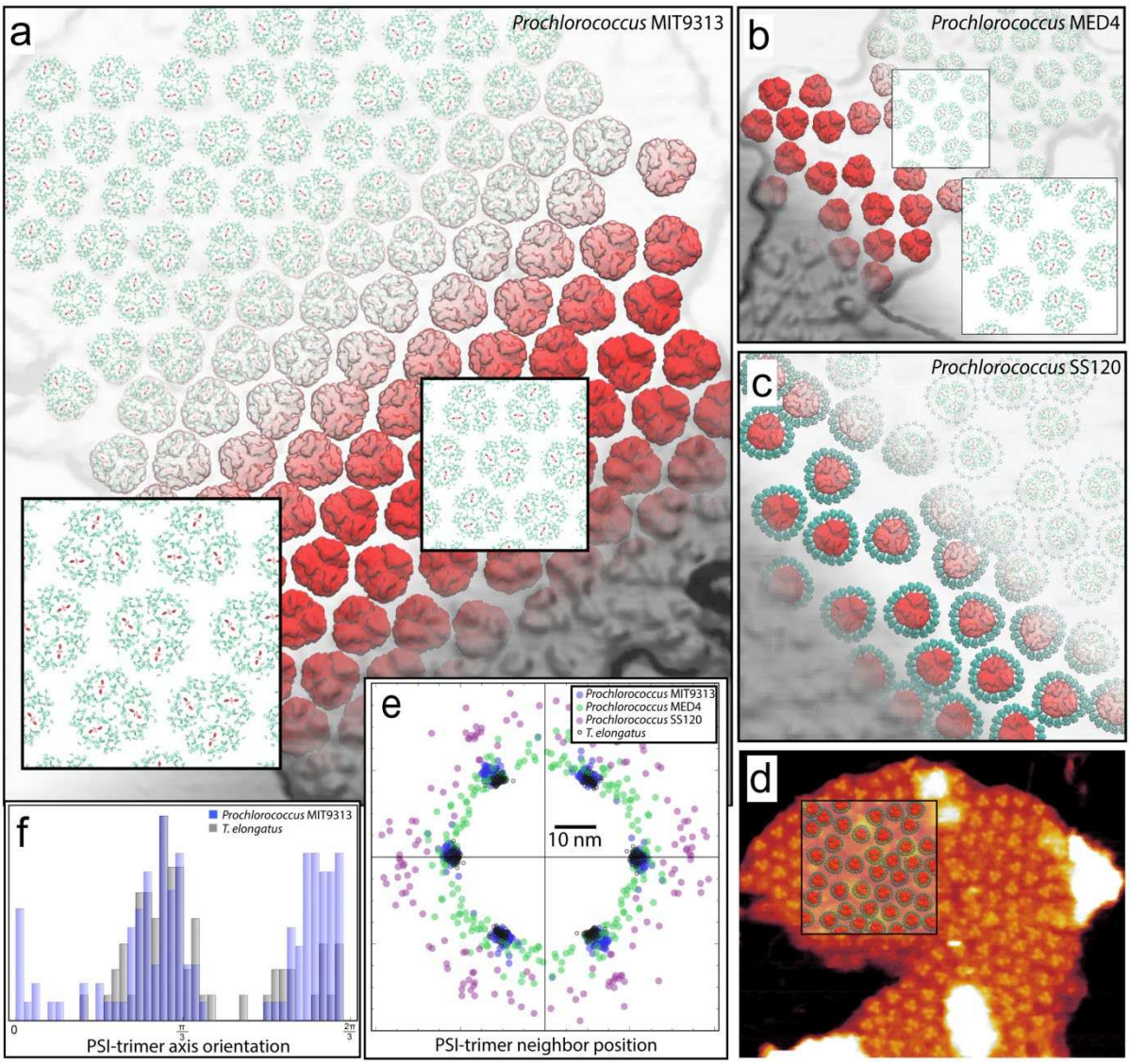

Fig. 6 Structural models for the PSI trimer domains from the *Prochlorococcus* ecotypes MIT9313, low-light grown MED4, and SS120. The models for MIT9313 (a), MED4 (b), and SS120 (c) domains are arranged according to AFM topographs from Figs. 2b, 1a, and 4a, respectively. The protrusions of the PsaC-D-E subunits of PSI trimers (red), modelled according to PDB ID: 1JB0[41], can be seen to correspond to AFM topological features (grey). Pcb units (blue) surrounding the PSI trimers in SS120 are modelled after CP43, PDB ID: 3WU2[44]. Constituent Chls are represented as porphyrin rings (red: PSI reaction center; green: PSI antenna; blue: Pcb (SS120 only)). The insets in (a) and (b) show typical Chl packing patterns, which for MIT9313 (a) reveal an arrangement similar to the one reported for *T. elongatus*[39] (see (e)). The relative location of the SS120 model (c) with respect to the AFM topograph of Fig. 4a is shown in (d). Long range order of PSI trimers is shown in (e) and (f) in terms of the neighbouring trimer positions and orientations, respectively, for the aforementioned ecotypes in comparison with *T. elongatus*[39]. The x-axis in (e) for each set is chosen arbitrarily for alignment purposes. The MIT9313 trimer spacings (blue) display a near-periodic arrangement resembling that of *T. elongatus* (grey circles); the MED4 (green) and SS120 (purple) ecotypes do not represent a periodic arrangement pattern for constituent proteins, with the spacing between PSI trimers in the SS120 ecotype being notably larger due to the presence of surrounding Pcb units. Orientational correlations

between PSI trimers are shown in (f) in terms of histograms for the angle between the symmetry axes of neighbouring trimers. Due to the C_3-symmetry of the trimer, only the region (0, 2π/3) is shown. The double peak for MIT9313 in contrast with *T. elongatus* shows a bi-modal distribution of orientation correlations, i.e., an arbitrary π/3 rotation of PSI trimers is more predominant in MIT9313 compared with *T. elongatus*. MED4 and SS120 trimer orientations do not display correlated behaviour and are therefore not shown. The models presented contain: MIT9313 (a): 133 PS1 trimers with 38,304 Chls; MED4 (b): 57 PS1 trimers with 16,416 Chls; SS120 (c): 42 PS1 trimers and 728 Pcb units with 21560 Chls.

Quantification of PSI, PSII, cytochrome b_6f, ATP synthase and Pcb proteins by mass spectrometry

The AFM analyses presented in Fig. 1-4 show the arrangements of individual complexes, with no averaging, in membranes patches, from samples retrieved from sucrose density gradients following treatment of thylakoids with digitonin. In all cases we observe closely packed PSI trimers, in some cases with a surrounding Pcb ring, but with no PSII and cytochrome b_6f complexes present. The packing density leaves no room for these complexes in the AFM topographs, yet they are required in a functioning photosynthetic cell. Thylakoid membranes adhere to the mica substrate in an orientation that displays the protruding cytoplasmic face of PSI; while this aids identification of PSI by AFM the poorly-protruding cytoplasmic faces of PSII and cytochrome b_6f complexes are difficult to identify. In order to obtain an averaged view of the composition of membranes prepared from the three *Prochlorococcus* ecotypes, we used analysis by mass spectrometry. The number (mean ± SD) of proteins identified in three replicate analyses of each ecotype was 864 ± 5 (high-light acclimated MED4), 781 ± 5 (low-light grown MED), 521 ± 9 (SS120) and 946 ± 11 (MIT9313). Label-free protein quantification of the complete data-set gave inter-replicate correlation coefficients of 0.993-0.999 (see Supplementary Fig. 2). Normalized ion counts for subunits PsaA and PsaB (PSI), PsbA and PsbB (PSII), PetA, PetB and PetC (cytochrome b_6f) and AtpF and AtpG (ATP synthase) are shown in Supplementary Table 1 and in Fig.7. As shown in Fig. 7, levels of PSI in thylakoids purified from the three ecotypes are all either close to or lower than the levels of PSII, with PSI:PSII ratios (expressed as monomer equivalents) of 1.11 (high-light grown MED4), 0.79 (low-light grown MED4), 0.97 (MIT9313) and 0.53 (SS120). A previous quantitative proteomic analysis of MED4 grown under a 24-hour light-dark illumination regime[WaldbauerRef] revealed a PSI:PSII ratio of 0.66 while the results of another study of SS120 cells cultured under constant blue light[Dom-MartinRef] gave a ratio of 1.19. Therefore, although deviation from the expected 1:1 PSI:PSII ratio for *Prochlorococcus* cells[25] is observable, PSI is not the dominant photosystem complex in *Prochlorococcus*, in marked contrast with model strains such as *Synechocystis* sp. PCC6803 and *Synechococcus* sp. PCC7002.

Fig. 7 also shows the levels of cytochrome b_6f and the ATP synthase in both the high-light acclimated MED4, low-light acclimated MED4, MIT9313 and SS120 membranes. The lowest level of the cytochrome b_6f complex was found in high-light MED4, only slightly less than that of SS120 ecotype. The cytochrome b_6f was detected at significantly higher levels in low-light ecotypes MED4 and MIT9313, approximately 3 times and 6 times that detected in the high-light acclimated MED4 sample. Furthermore, levels of cytochrome b_6f are positively correlated with PSI ($p < 0.00001$) and PSII ($p = 0.003$, see Supplementary Fig. 3), highlighting the functional linkage between these complexes. The levels of the ATP synthase were less variable between the ecotypes with the high-light MED4 cells

357 again having the lowest levels, approximately 2-fold higher in SS120 and approximately 3-fold higher
358 in MIT9313 and low-light grown MED4.

359

360 The different ecotypes of *Prochlorococcus marinus* contain a variety of Pcb protein isoforms encoded
361 within their genomes. MED4 only carries *pcbA* and the corresponding protein was detected in this
362 analysis in both the high and low light MED4 thylakoid membranes, with a three-fold higher level in
363 low light membranes (Fig. 8). MIT9313 carries both *pcbA* and *pcbB*, but MS analysis detected only the
364 latter isoform and at less than half of the PcbA level of MED4. The genome of encodes SS120 has eight
365 Pcb isoforms and all except PcbC were detected, giving a combined Pcb level 7.0- 2.2- and 3.6-fold
366 greater than that in high- and low-light MED4, and MIT9313 respectively. The ratio of combined-
367 Pcb:PSI was 2.08, 1.89, 0.66 and 5.74 in in high-light MED4, low-light MED4, MIT9313 and SS120
368 respectively.

369

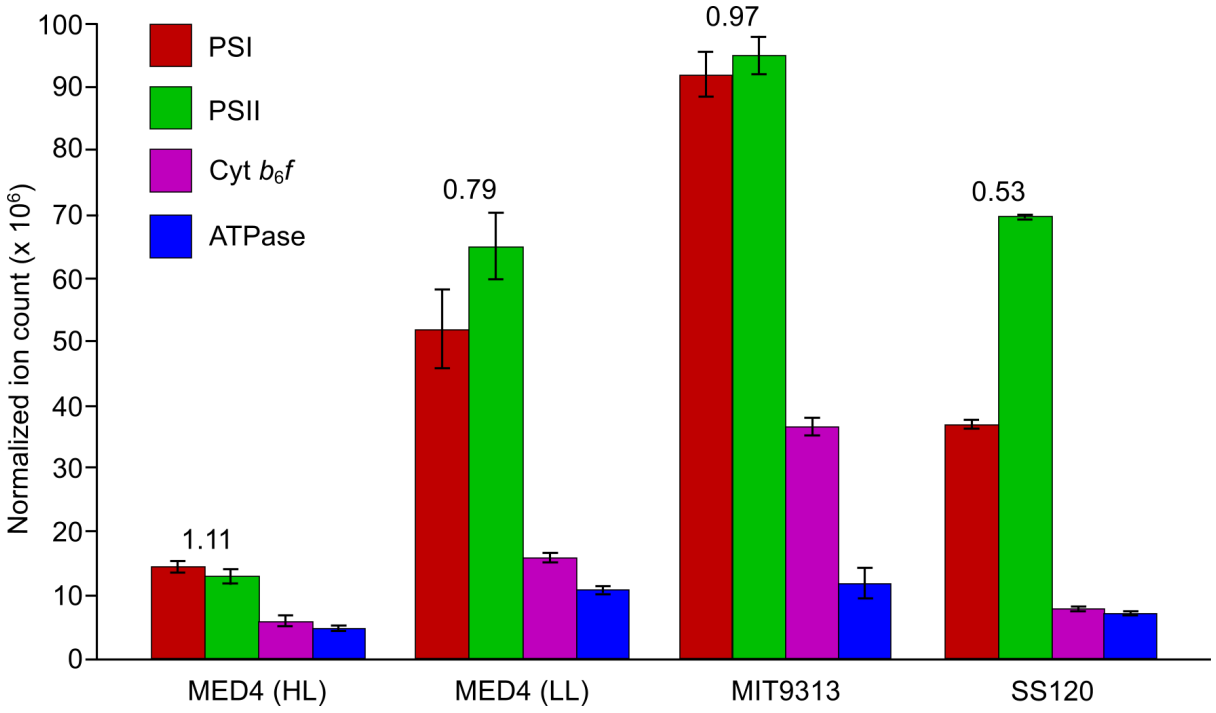

370

371

372 **Fig. 7 Comparison of the relative levels of PSI, PSII, cytochrome *b_6f* and ATP synthase in**
373 ***Prochlorococcus marinus* ecotypes MED4, MIT9313 and SS120.** Proteins extracted from thylakoid
374 membranes were analysed by mass spectrometry and quantified by the iBAQ method (see Materials
375 and Methods). MED4 was grown under both high light (HL) and low light (LL). MIT9313 and SS120
376 were grown under low light. Levels of PSI, PSII, cytochrome *b_6f* and ATP synthase were calculated from
377 the sum of the normalized ion counts (see Supplementary Table 1a-c) of subunits PsaA and PsaB (PSI),
378 PsbA and PsbB (PSII), PetA, PetB and PetC (Cyt *b_6f*), AtpF and AtpG (ATPase). These subunits were
379 selected as representative of their respective protein complexes owing to their detection in all
380 analyses. Means and SDs (n = 3 technical replicates) are shown together with PSI:PSII ratios which are
381 displayed above the PSI and PSII.

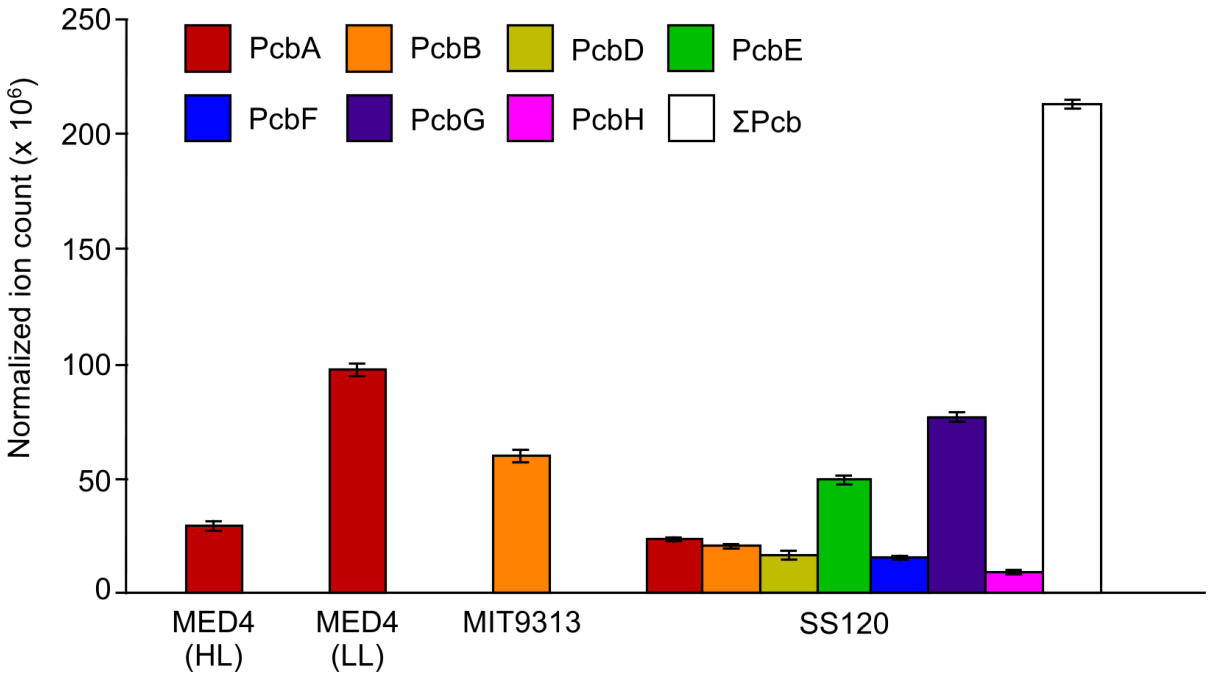

Fig. 8 Profiles of Pcb proteins expressed in *Prochlorococcus marinus* ecotypes MED4, MIT9313 and SS120. Proteins extracted from thylakoid membranes were analysed by mass spectrometry and quantified by the iBAQ method (see Materials and Methods). The normalized ion counts (see Supplementary Table 1, a-c) of the divinyl chlorophyll a/b light-harvesting protein isoforms identified are shown as means and SDs (n = 3). PcbA is the only Pcb isoform present in MED4. Although MIT9313 contains both *pcbA* and *pcbB* in its genome, only PcbB was identified. For the SS120 ecotype, in which 7 out of a total of 8 Pcb isoforms were identified (PcbC was not detected, as in a previous study[26]), the sum of all Pcb ion counts is also shown

Quantification of the Chl content of *Prochlorococcus* ecotypes MED4, MIT9313 and SS120

Chl *b:a* ratios in the thylakoid membranes purified from high-light acclimated MED4, low-light acclimated MED4, MIT9313 and SS120 were determined from reverse-phase HPLC of methanol-extracted pigments. Chl *a* and Chl *b* were separated (Supplementary Fig. 4) and collected before being buffer exchanged into 90% acetone. The amount of Chl *a* was calculated from the absorption at 663 nm using the molar extinction coefficient[45] of 78.75 x 10^3 $M^{-1}.cm^{-1}$ and the amount of Chl *b* was calculated from the absorption at 647 nm using the molar extinction coefficient[45] 46.61 x 10^3 $M^{-1}.cm^{-1}$. The Chl *b:a* ratios were 0.06, 0.27, 1.52 and 2.36 for thylakoid membranes from high-light MED4, low-light MED4, MIT9313 and SS120 respectively (Fig. 8a). In each pigment extract the combined Chl *a* and *b* concentration was calculated to be 26.6, 62.5, 115.8 and 91.4 µg Chl per mg of protein in high-light MED4, low-light MED4, MIT9313 and SS120 respectively (Fig. 8b).

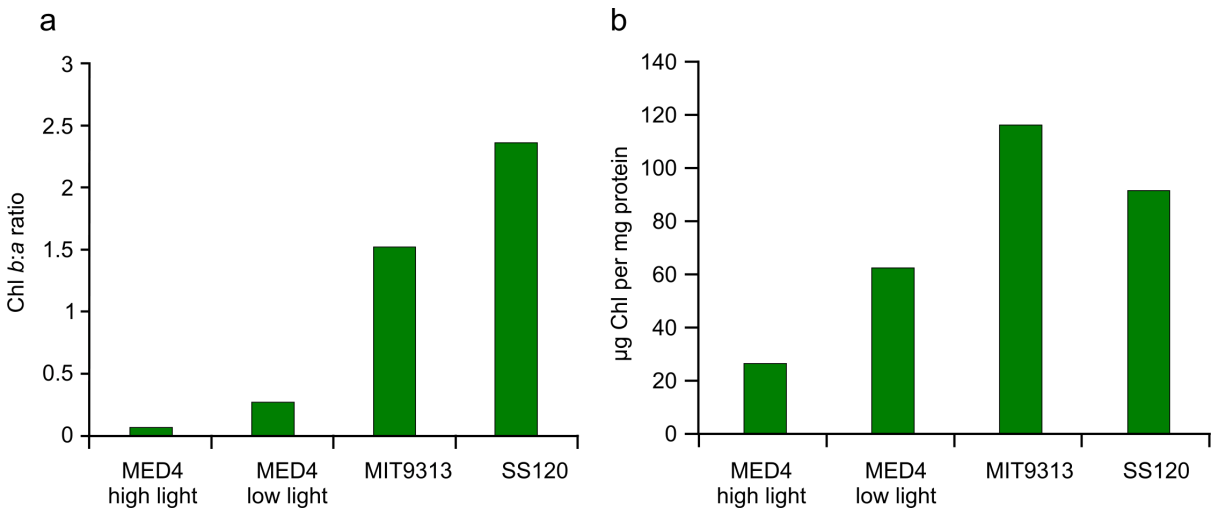

Fig. 9 Chl *b*:*a* ratio in *Prochlorococcus marinus* ecotypes MED4, MIT9313 and SS120 determined by reverse-phase HPLC. Chl *a* and Chl *b* in pigment extracts of thylakoid membranes from high-light acclimated MED4, low-light acclimated MED4, MIT9313 and SS120 cells were separated by reverse-phase HPLC. For each ecotype the Chl *b*:*a* ratio (a) and the combined Chl *a* and Chl *b* per mg of protein (b) are displayed.

Discussion

Identification of domains of PSI complexes in *Prochlorococcus* ecotypes

Previous studies have shown that AFM can be used to identify photosystems in oxygenic phototrophs, and to determine their organisation in thylakoid membranes[30-36,39,40]. The most accurate measurement recorded by the AFM is the distance measured in the Z-plane, henceforth referred to as the height, which is typically accurate to 0.1 nm. The average heights measured for complexes in MED4 and MIT9313 membranes, and the average lateral distance between monomers, are consistent with both the crystal structure of the PSI trimer (PDB ID:1JB0) and previous measurements of PSI in thylakoid membranes[39], allowing the identification of these complexes as trimeric PSI. This study[39] found that the lumenal face of PSI-rich cyanobacterial thylakoids generally adsorbed to the mica substrate, which, in terms of AFM imaging, favours the marked topographic features of PSI over the low-topology PSII and cytochrome b_6f complexes on the cytoplasmic face of the membrane. The same constraints apply to the topographs of *Prochlorococcus* membranes reported herein; thus, despite the abundance of PSII in all three ecotypes revealed by our MS analyses, PSI-rich membrane domains feature in Fig. 1-5. The close packing and high density of PSI complexes in these domains, whether as trimers (Fig. 1, 2, 3, 6a, 6b) or in supercomplexes with a Pcb antenna ring (Fig. 4, 5, 6c), leaves no room for either PSII or cytochrome b_6f complexes, which must reside in other domains of the thylakoid system. The presence of PSI-enriched areas of membrane is consistent with previous studies of thylakoid membranes from cyanobacteria and stromal lamellae in plant chloroplasts. These arrangements of PSI could optimise energy trapping and electron transport in these organisms, for example to mitigate 'spillover' of excitation energy (REF)when PSI and PSII are in close proximity (REF). The segregation of PSI from PSII in large domains is believed to be an adaptation that plants (REF), algae (Engel et al.,

434 2015), cyanobacteria (MacGregor-Chatwin et al., 2017) and now *Prochlorococcus* appear to employ to
435 ensure efficient PSII function. Another aspect of electron transport to consider is that the larger the
436 PSI domains are, the further reduced plastocyanin molecules must diffuse from the cytochrome b_6f
437 complex in order to deliver electrons to the acceptor side of the PSI complex, which will change the
438 rate at which linear electron flow takes place. The same is true for the diffusion of ferredoxin for the
439 purposes of cyclic electron transport; it is possible that the size of the PSI domains in *Prochlorococcus*
440 ecotypes optimises the balance between linear and cyclic electron flow to control its production of
441 ATP and NADPH depending on its metabolic needs of the organism. For example, has been shown in
442 plants that differences in the size of grana, which predominantly contain PSII and the cytochrome b_6f
443 complex, can have a marked effect on cyclic and linear electron flow (Wood et al. 2018). However,
444 further elucidation of organisation of PSII and the cytochrome b_6f complex is required before
445 conclusions can be drawn on cyclic and linear electron flows in *Prochlorococcus* and other
446 cyanobacteria

447 As discussed above, this *Prochlorococcus* study did not identify membrane domains where PSI is
448 interspersed with other photosynthetic complexes such as PSII, possible because the lumenal face of
449 PSI-rich membranes tends to adsorb efficiently to the mica substrate used for AFM imaging. In
450 contrast, previous studies did identify and image thylakoid membrane regions in *T. elongatus* and
451 *Synechococcus* 7942 where PSI complexes co-localise with PSII and the cytochrome b_6f complex[39,40].
452 Mass spectrometry analysis of thylakoids from *Prochlorococcus* ecotypes did however detect peptides
453 from these two protein complexes; the PSI:PSII ratios in thylakoids from high-light acclimated MED4,
454 low-light acclimated MED4, MIT9313 and SS120 cells were 1.11, 0.79, 0.97 and 0.53, respectively. The
455 lower PSI:PSII ratio in SS120 membranes could be a consequence of the membrane area occupied by
456 Pcb proteins , thereby decreasing the space available for PSI.

457

458 **MED4**

459 Imaging the native membrane arrangements of PSI and other complexes in *Prochlorococcus* ecotypes
460 provides an opportunity to calculate membrane densities of PSI complexes and chlorophyll pigments;
461 in the case of the high-light adapted MED4 we were also able to compare the effects of growing the
462 cells at 5 and 250 µmol photons m^{-2} s^{-1}. This higher figure is lower than irradiances experienced by
463 MED4 in surface waters (ref), but it is close to the limit we could achieve for laboratory-grown cultures.
464 The averages for membrane packing density of PSI and chlorophyll for low-light MED4 were 4303 and
465 411590 per μm^2, respectively and the averages for high-light MED4 were 3553 and 341120 per μm^2.
466 At both light intensities the PSI domains imaged in this ecotype had a somewhat random distribution
467 and were loosely packed in the thylakoid membrane, reminiscent of PSI organisation in *Synechocystis*
468 sp. PCC 6803[39] and *Synechococcus* sp. PCC 7942[40]. The major difference between the two light
469 conditions is the five-fold increased prevalence of monomeric or dimeric PSI in high light. The reasons
470 for this are unclear, although it has been shown in thylakoid membranes from other cyanobacteria
471 the probability that light energy absorbed by a PSI monomer within a trimeric complex has a
472 probability of 0.35 of being trapped by a neighbouring monomer[39]. Adapting to high light conditions
473 could require not only a lower packing density of PSI within the membrane, but also a switch away
474 from a trimeric configuration. At lower light intensities there is greater need for efficient energy
475 harvesting and very densely packed PSI complexes as well as a mimimal number of monomers and

476 dimers, as seen here for the low light-adapted MIT9313 ecotype, could confer an advantage at lower
477 irradiances..

478 The MED4 strain is most abundant in surface waters of the open ocean[15]; closer to the surface of the
479 ocean there is greater irradiance, so HL-adapted ecotypes such as MED4 do not need to waste
480 metabolic resources by packing their thylakoid membranes full of chlorophyll-containing proteins.
481 Whilst having a greater light harvesting capacity could confer a competitive advantage, the
482 oligotrophic waters that the MED4 strain occupies are very low in nutrients and synthesising
483 photosynthetic reaction centres is costly to the cyanobacterium in terms of nitrogen and iron. It is
484 likely that the markedly lower concentration of photosystems in this strain relative to the LL-adapted
485 MIT9313 strain is a result of having to balance the need to absorb light energy with the metabolic
486 requirements of producing photosystem complexes. The mass spectrometry data would seem to
487 support this hypothesis as we see a large reduction in the levels of PSI, PSII, cytochrome b_6f and Pcb
488 proteins in high-light grown MED4 relative to low light.

489 The higher chlorophyll *b*:*a* ratio measured for low-light MED4, and much higher value for the MIT9313
490 and SS120 ecotypes is in keeping with the idea that chlorophyll *b* is utilised more extensively by LL
491 adapted strains. Having more chlorophyll *b* increases spectral coverage in the blue region of the
492 spectrum, which is the only light present deeper in the euphotic zone that these ecotypes occupy.

493

494 **MIT9313**

495 In contrast to MED4, the thylakoids of the LLIV ecotype MIT9313 contain domains that consist of
496 densely packed PSI complexes, organised into pseudo-hexagonal arrays very similar in size and
497 appearance to those previously imaged in *T. elongatus*[39] and suggesting that this type of crystalline
498 packing of PSI may be a common membrane motif across many different species of cyanobacteria.
499 MIT9313 thylakoids (Fig. 2) had average PSI and chlorophyll densities of 5583 and 536044 per μm^2
500 respectively.

501 The structural model of the MIT9313 membrane, based on AFM data (Fig. 5a,e), showed that MIT9313
502 features a near-identical packing pattern to that of *T. elongatus*[39]. This previous study allowed
503 calculation of the probability that harvested excitation energy is either trapped within a particular
504 trimer (0.35), or that it can migrate to another trimer (0.07)[39]. Thus, it appears that the main point of
505 having tightly packed PSI complexes is not to create inter-trimer energy transfer networks, but simply
506 to achieve the highest possible density of chlorophyll pigments in the thylakoid membranes. We
507 speculate that these more densely packed PSI domains in MIT9313 are an adaptation to the lower
508 light conditions and the higher availability of nutrients in the deeper euphotic zone[16]. With iron and
509 nitrogen less scarce in this zone the cost of synthesising photosystems becomes less severe and the
510 cyanobacteria are able to produce more PSI relative to their HL-adapted counterparts. By packing PSI
511 in a pseudo-hexagonal lattice MIT9313 gains a competitive advantage in the LL environment of the
512 lower euphotic zone.

513 AFM images those membranes that adhere to the mica substrate, and the analysis is limited by the
514 number of membranes that can be examined. Mass spectrometry of the purified thylakoids provides
515 a more complete picture of the differences in PSI abundance between MIT9313 and MED4, and it

516 shows that there is an approximately six-fold increase in PSI and nine-fold more PSII in MIT9313. Using
517 cryo-EM tomography data obtained for MED4 and MIT9313[29] it was possible to estimate that these
518 HL-adapted and LL-adapted ecotypes contain ~6 μm^2 and ~22 μm^2 of thylakoid membrane area,
519 respectively. Considering that there are 1.8 times as many PSI complexes in MIT9313 thylakoid
520 membranes per unit area and cells house approximately 3.7-fold more membrane, each MIT9313 cell
521 could house as much as 6.7 times the number of PSI complexes relative to the HL-adapted MED4
522 ecotype. Pigment analysis showed that thylakoid membranes from MIT9313 had significantly more
523 chlorophyll per mg of protein than MED4 and SS120 (Fig. 8b); supporting the hypothesis that MIT9313
524 has adapted to low light by maximising the number of pigments in the thylakoid membrane.

525

526 **SS120**

527 This ecotype employs a different strategy to combat the limitations of low light levels, and we found
528 a different organisation of PSI in the LLII strain SS120; it was possible to image densely packed Pcb-PSI
529 supercomplexes confirming the structures of isolated complexes[25] and additionally showing the
530 organisation of these supercomplexes in the native membrane environment. SS120, which has
531 abundant Pcb proteins (Fig. 8), contains large membrane domains comprising hundreds of trimeric PSI
532 complexes, with each trimer surrounded by a multi-subunit ring (Fig. 4, 5); these complexes are very
533 similar in appearance and dimensions to the Pcb-PSI supercomplex[25,26] and were assigned as Pcb-PSI
534 supercomplexes. The SS120 membrane patch measured in Fig. 5 contained 893 Pcb-PSI
535 supercomplexes per μm^2, with 2679 PSI complexes per μm^2 and 498294 chlorophyll pigments per
536 μm^2, assuming 15 Chl molecules per Pcb protein. This 52% reduction in the levels of PSI in SS120
537 relative to MIT9313 is in good agreement with the mass spectrometry analysis of purified theylakoids
538 which reveals a 59% reduction in the total number of PSI complexes. Relative to MIT9313, adaptation
539 to low light in SS120 appears to involve the synthesis and assembly of fewer PSI reaction centres and
540 filling the membrane area gained with Pcb light-harvesting complexes. This strategy is likely to require
541 a lower energy input for biosynthesis, given the lower ratio of proteins to be synthesised per bound
542 pigment (kDa/pigment) in antenna proteins generally, with respect to reaction centre complexes. For
543 the Pcb proteins found in *Prochlorococcus*, assuming similarity with IsiA proteins, which bind 15 Chls,
544 this ratio was estimated to be 2.6, whereas it is 6.5 for marine cyanobacterial phycoerythrin, and 3.7
545 for cyanobacterial PSI[22]. Thus, a combination of nitrogen and light limitation disfavours
546 phycobilisomes and favours Pcb antenna complexes, in *Prochlorococcus* SS120 at least. These features
547 of SS120 confer significant competitive advantages over other picoplankton, allowing this ecotype to
548 thrive in low nutrient oligotrophic waters found in the open ocean[5]. Another adaptation of SS120 to
549 low light is the deployment of an increased number of Chl *b* pigments. Pigment analyses show that
550 the Chl *b*:*a* ratio of SS120 membranes is ~40-fold higher than for than for high-light grown MED4 (Fig.
551 9). This increased level of Chl *b* gives SS120 greater access to the blue regions of the solar spectrum
552 that represent the only light available at a depth of 200 meters[18]. The above considerations also apply
553 to the formation of Pcb-PSII complexes, although the membrane regions housing them were not
554 imaged in the present study. Finally, the positive correlation between levels of PSI and cytochrome b_6f
555 complexes, and the increased proportion of PSII that emerged from mass spectrometry analysis of
556 SS120 might reflect an adaptation to life in iron-deficient environments. Both PSI and cytochrome b_6f
557 complexes place demands on the supply of iron, whereas PSII has a lower iron requirement.

558 Mass spectrometry analysis of SS120 thylakoid membranes also highlighted the presence of
559 approximately 7.0, 1.8 and 3.5 times more total Pcb proteins relative to high-light MED4, and MIT9313
560 membranes respectively. It has been reported that the Pcb-PSI supercomplex comprises an 18-
561 membered ring of PcbG[25,26]; in agreement with this analysis, our MS data shows that PcbG is the most
562 abundant Pcb protein in SS120, and thus likely the identity of the Pcb subunits imaged in Fig. 3. The
563 presence of 6 other Pcb proteins is consistent with previous analysis of the antenna complexes in
564 SS120 cells[26]. It has been shown that PcbA acts as an antenna for the PSII complex and PcbG and PcbC
565 can make up the ring surrounding trimeric PSI complexes[26]. Despite the presence of the *pcbC* gene in
566 this ecotype the PcbC protein could not be detected. PcbC is involved in the iron starvation response
567 in SS120, where it replaces the PcbG protein in the 18 membered ring around the PSI trimer[26].
568 However, the SS120 cells studied in the present work were not grown under iron starvation conditions,
569 which accounts for the absence of PcbC from our mass spectrometry analysis. Although present in the
570 cell, the functions of the other Pcb proteins, PcbB, D, E, F, H, are unknown. However, it is interesting
571 to note that the ratio of total Pcb:PSI is 5.74; close to the ratio of 6 required for a Pcb-PSI supercomplex
572 composed of 18 Pcb proteins and 3 PSI complexes. This similarity could imply that these other Pcb
573 proteins are involved in forming Pcb-PSI supercomplexes, but this interpretation must be viewed with
574 caution as it has been shown that a certain population of Pcb proteins associates with PSII in this
575 ecotype (min chen and Bibby ref). It is likely that there is a population of PSI complexes that are not
576 associated with an Pcb ring, which we were not able to image with AFM.

577 In conclusion, we have presented the first high resolution imaging of the photosystems in the thylakoid
578 membranes from one HL-adapted ecotype and two LL-adapted ecotypes of the globally important
579 cyanobacterium, *Prochlorococcus*. The AFM topographs were used as the basis for constructing
580 structural models of PSI-rich domains of thylakoids from *Prochlorococcus* ecotypes, MED4, MIT9313
581 and SS120 that reveal the packing patterns of PSI complexes. Additionally we have used mass
582 spectrometry to quantify the major photosynthetic protein complexes in each ecotype. The
583 organisation and composition of thylakoid membranes can be related to the particular environmental
584 niches occupied by each ecotype. Whilst this is the first step in understanding the architecture of the
585 photosynthetic membrane system in *Prochlorococcus* there are still several questions that remain
586 unanswered, including the organisation of PSII and the cytochrome b_6f complexes. It has been shown
587 that Pcb proteins act as antenna complexes for PSII but how these supercomplexes associate in the
588 membrane environment is still unclear, as are the structures of the various Pcb proteins. With such
589 knowledge, it would be possible to build a functional model of the complete photosynthetic
590 membrane system in one of the most important photosynthetic organisms.

591

592

593

594

595

596

597

598 **Materials and methods**

599 **Cell growth**

600 *Prochlorococcus* spp. MED4, SS120 and MIT9313 were grown at 22°C in PCR-S11 medium[46] at a white
601 light intensity of 5 µmol photons m^{-2} s^{-1}. Cells were harvested by centrifugation at 10000 rpm using a
602 JA-25.50 rotor (Beckman) at 20°C for 30 minutes and flash frozen in liquid nitrogen before storing at -
603 80°C for subsequent membrane isolation. High light growth conditions

604 **Crude membrane preparation**

605 A volume of 1.0 ml of resuspended cells was added to 1.0 ml of glass beads and cells were broken by
606 6 rounds of bead beating for 30 seconds in a Mini bead beater (Biospec products). The cell lysate was
607 removed from the glass beads by pipette and then layered onto a 11.5 ml sucrose step gradient
608 composed of 9.5 ml of 30% (w/w) sucrose on a 2.0 ml 50% (w/w) sucrose cushion. The sucrose gradient
609 was then centrifuged at 30000 rpm in an SW41 rotor (Beckman) at 4 °C for 30 minutes. The thylakoid
610 membranes were present at the interface between the 30% and 50% (w/w) sucrose volumes, which
611 were harvested and either immediately used for AFM analysis or were flash frozen in liquid nitrogen
612 and then stored at -80 °C for later use

613 **Preparation of membranes for AFM analysis**

614 Harvested crude membranes were loaded onto 11.5 ml continuous sucrose gradients made from
615 equal volumes of 20% and 50% (w/w) sucrose which contained 0.1% digitonin (w/w). These sucrose
616 gradients were centrifuged at 40000 rpm in an SW41 rotor (Beckman) at 4°C for 2 hours. The thylakoid
617 membranes were present as a green smear running roughly the length of the gradients; membranes
618 were harvested from throughout the gradient and used for AFM analysis.

619 **AFM imaging**

620 **Instrumentation**

621 Membrane samples were imaged using a multimode VIII AFM with a Nanoscope 8.0 controller (Bruker
622 Nano Surfaces Business).

623 **Sample adsorption**

624 Approximately 5 µl of membrane sample was pipetted onto a freshly cleaved mica substrate before
625 45 µl of buffer containing 10 mM HEPES pH 7.5 and 100 mM KCl was pipetted onto the mica. The
626 membranes were incubated for 1 hour before being washed 3 times with 50 µl of the same buffer,
627 with the final wash left on the surface. The mica disk was then mounted onto the (J-scanner) AFM
628 scanner.

629 **Sample imaging**

630 Samples were imaged using Peak Force Nanomechanical Mapping™ (PF-QNM) mode under liquid
631 using a Peak Force frequency of 2 kHz. An SNL AFM probe (Bruker Nano Surfaces Business) mounted
632 in a MTFML fluid cell (Bruker Nano Surfaces Business) was used to image membrane samples. Once
633 the probe had been loaded into the fluid cell the reservoirs were filled with buffer containing 10 mM

634 HEPES pH 7.5 and 100 mM KCl and the cell was mounted onto the AFM at which point the laser was
635 aligned with the probe. A Peak Force amplitude of 5-20 nm was used and images were taken at
636 256 x 256 or 512 x 512 pixels. The force imparted on the sample during imaging was varied between
637 5-1000 pN and image processing was performed using NanoScope Analysis 1.9 or Gwyddion v2.47[47].
638 Heights and distances are expressed as the mean ± the standard deviation.

639 **Construction of structural models for *Prochlorococcus* MIT9313, MED4, SS120 ecotypes**

640 The construction of structural models for PSI containing thylakoid membranes, based on AFM
641 topographs, follows the protocol employed earlier for *T. elongatus* PSI domains[39]. Specifically, the
642 crystal structure, PDB:1JB0[41] of PSI trimers from *T. elongatus* is used to match the protrusion profiles
643 of PsaC-D-E subunits onto the topological features revealed by AFM. *Mathematica*[48] was employed
644 with image recognition methods to determine the position and orientation of each trimer with respect
645 to the AFM density. The structural models were manually refined iteratively using VMD[49]. For ecotypes
646 MIT9313 (Fig. 5a) and MED4 (Fig. 5b), the corresponding structural models contain only PSI-trimers,
647 whereas for SS120 (Fig. 5c) the membrane domain contains also surrounding Pcb units modelled in
648 terms of CP43, PDB ID: 3WU2[44]. Even though the structural models show atomistic detail (Figs. 5a, 5b,
649 5c) as determined by the underlying crystal structures[41,44], the resolution of the models should be
650 considered to be limited by the native AFM resolution, namely, 9.9 Å, 14.6 Å, 18.6 Å, for MIT9313 (Fig.
651 5a), MED4 (Fig. 5b), and SS120 (Fig. 5c) models, respectively. Excitonic connectivity between PSI
652 subunits in a thylakoid membrane was calculated on an effective Hamiltonian formulation[39,50].

653 **Proteomic analysis of thylakoid membranes**

654 Thylakoid membranes (50 µg protein) from *Prochlorococcus marinus* ecotypes MED4, SS120 and
655 MIT9313 were processed using a 2-D clean-up kit (GE Healthcare) to isolate the proteins from lipids
656 and cofactors. The extracted proteins were solubilized, S-alkylated, digested and analysed by nano-
657 flow liquid chromatography coupled to mass spectrometry as previously described[51]. Tryptic peptides
658 were resolved using a 3-hour gradient and the mass spectrometer was programmed for data
659 dependent acquisition with 10 product ion scans (centroid, resolution 15000, automatic gain control
660 5e4, maximum injection time 20 ms, isolation window 1.2 Th, normalized collision energy 32, intensity
661 threshold 2.5e5) per full MS scan (profile, resolution 60000, automatic gain control 3e6, maximum
662 injection time 100 ms). Protein identification was carried out using MaxQuant v. 1.5.3.30[52] to search
663 the *Prochlorococcus marinus* reference proteome databases for ecotypes: (1) MED4
664 (www.uniprot.org/proteomes/UP000001026, 1924 proteins, downloaded on 17-03-16), (2) SS120
665 (www.uniprot.org/proteomes/UP000001420, 1881 proteins, downloaded on 17-03-16), (3) MIT9313
666 (www.uniprot.org/proteomes/UP000001423, 2830 proteins, downloaded on 31-10-16). Default
667 database search parameters were used and protein quantification was enabled by selecting the iBAQ
668 option (Intensity-Based Absolute Quantification, a widely accepted and validated label-free protein
669 quantification method[51,52]). Identification and quantitative results were further processed using
670 Perseus software v. 1.5.3.2[53]. Protein amounts were normalized to compensate for random variation
671 in sample loadings and tryptic peptide spectral acquisition patterns by applying a factor derived from
672 the ion intensity of the trypsin auto-digestion peptide VATVSLPR (Li et al 2016) (see Supplementary
673 Table 2) present in all analyses.

674

675 **Pigment analysis**

676 Membrane samples (140 µg protein) were pelleted by centrifugation at 270000 x g at 4 °C for 1 hour.
677 Chlorophylls were extracted from membrane pellets by addition of 100 µl methanol and vortexing at
678 room temperature under dim green light. The extracted pigments were separated from insoluble
679 material by centrifugation (15,000 rpm, 4°C, 15 mins) and 80 µl of the supernatant was immediately
680 analysed by reverse phase high performance liquid chromatography (HPLC) on an Agilent 1200 HPLC
681 system using a Discovery® HS C18 5 µm column (column dimensions: 25 cm × 4.6 mm) pre-equilibrated
682 in 84:9:7 acetonitrile:methanol:water (solvent A). Pigments were separated at a solvent flow rate of
683 1 ml min^{-1} using a mobile phase consisting of solvent A and solvent B (68:32 methanol:ethyl acetate)
684 and a linear gradient from 100% solvent A to 100% solvent B over 12 minutes followed by isocratic
685 elution with 100% solvent B for 6 minutes[56]. The column was re-equilibrated with 100% solvent A for
686 6 minutes prior to injection of the next sample. Absorbance was monitored at 653 nm and 663 nm
687 using a diode-array detector; divinyl-chlorophyll *b* (DV-Chl *b*) and divinyl-chlorophyll *a* (DV-Chl *a*)
688 eluted at ~13.8 minutes and ~15.3 minutes, respectively, as determined by their absorbance spectra.

689 Collected Chl *a* and Chl *b* solutions were placed in an Eppendorf concentrator plus and centrifuged
690 under vacuum until the solvent evaporated. The solid pigments were then resuspended in 90% (v/v)
691 acetone and the Chl *a* content was calculated from measuring the absorption at 664 nm using the
692 extinction coefficient of 78.75 x 10^3 $M^{-1}.cm^{-1}$. The Chl *b* content was calculated using the absorption
693 at 647 nm using an extinction coefficient of 46.61 x 10^3 $M^{-1}.cm^{-1}$ respectively[45]. All absorption spectra
694 were taken using a Cary 60 (Agilent technologies).

695 **Protein content calculation**

696 The protein concentration of samples was calculated as previously described[57].

697 **Purification of IsiA-PSI supercomplexes**

698 IsiA-PSI supercomplexes were purified as previously described[27].

699 **TEM imaging**

700 A solution containing IsiA-PSI supercomplexes was pipetted (~20 µl) onto a charged carbon coated
701 grid and incubated for 2 minutes. The sample was negatively stained with 0.75% w/v uranyl formate
702 and imaged with a Philips CM100 microscope that was equipped with a Gatan Ultrascan 667 CCD
703 camera. Particles were viewed with magnification of x1000- x52000. 52 particles were chosen from a
704 field of IsiA-PSI supercomplexes observed by negative stain TEM and image processing was performed
705 by Digital Micrograph (Gatan. Inc.) and the IMAGIC-5 image processing system

706

707 **Acknowledgements**

708 This work was supported by Advanced Award 338895 from the European Research Council which
709 funded CM-C, PJJ, JWC, PQ and provided partial support for CNH. CNH and AH also gratefully
710 acknowledges financial support from the Biotechnology and Biological Sciences Research Council
711 (BBSRC UK), award number BB/M000265/1. CNH, MS and ZLS were supported by the Photosynthetic
712 Antenna Research Center (PARC), an Energy Frontier Research Center funded by the U.S. Department

of Energy, Office of Science, Office of Basic Energy Sciences under Award Number DE-SC 0001035. MS and ZLS were also supported by the National Science Foundation (MCB1616590) and the National Institutes of Health (NIH 9P41GM104601) DJS acknowledges funding from NERC (NE/N003241/1) and The Leverhulme Trust (RPG-2014-354). MJD acknowledges support from the Biotechnology and Biological Sciences Research Council (UK) (BB/M012166/1). MPJ would like to acknowledge BBSRC Grant BB/P002005/1 and the Grantham Centres for Sustainable Futures, University of Sheffield, for G.E.M.'s studentship.

Author contributions

CM-C, DJS and CNH designed the research. CM-C, PJJ, MS, JWC, AH, PQ, MJD, GEM and DJS performed the research. CM-C, MS, MPJ, ZLS and CNH wrote the paper.

References

1. Flombaum, P., Gallegos, J. L., Gordillo, R. A., Rincón, J., Zabala, L.L., Jiao, N., Karl, D. M., Li, W. K., Lomas, M. W., Veneziano, D. and Vera, C. S., 2013. Present and future global distributions of the marine Cyanobacteria *Prochlorococcus* and *Synechococcus*. *Proc. Natl Acad. Sci* USA **110**, pp.9824-9829 (2013).

2. Huston, M. A. & Wolverton, S. The global distribution of net primary production: resolving the paradox. *Ecol. Monographs* **79**, 343–377 (2009).

3. Partensky, F. & Garczarek, L. *Prochlorococcus*: Advantages and limits of minimalism. *Annu. Rev. Marine. Sci.* **2**, 305–331 (2010).

4. Goericke, R. & Repeta, D. J. The pigments of *Prochlorococcus marinus*: the presence of divinyl chlorophyll *a* and *b* in a marine procaryote. *Limnol. Oceanogr.* **37**, 425–433 (1992).

5. Partensky, F., Hess, W. R. & Vaulot, D. *Prochlorococcus*, a marine photosynthetic prokaryote of global significance. *Microbiol. Mol. Biol. Rev.* **63**, 106–127 (1999).

6. Partensky, F., Hoepffner, N., Li, W. & Ulloa, O. Photoacclimation of *Prochlorococcus* sp. (Prochlorophyta) strains isolated from the North Atlantic and the Mediterranean Sea. *Plant Physiol.* **101**, 285–296 (1993).

7. Moore, L. R., Goericke, R. & Chisholm, S. W. Comparative physiology of *Synechococcus* and *Prochlorococcus*: influence of light and temperature on growth, pigments, fluorescence and absorptive properties. *Marine Ecol. Progress Series* **116**, 259–275 (1995).

8. Moore, L. R. Goericke, R & Chisholm, S. W. Physiology and molecular phylogeny of coexisting *Prochlorococcus* ecotypes. *Nature*, **393,** 464-467 (1998).

9. Ferris, M. J. & Palenik, B. Niche adaptation in ocean cyanobacteria. *Nature* **396**, 226–228 (1998).

10. Urbach, E., Scanlan, D. J., Distel, D. L., Waterbury, J. B. & Chisholm, S. W. Rapid diversification of marine picophytoplankton with dissimilar light-harvesting structures inferred from sequences of *Prochlorococcus* and *Synechococcus* (Cyanobacteria). *J. Mol. Evol.* **46**, 188–201 (1998).

11. West, N. J. & Scanlan, D. J. Niche-partitioning of *Prochlorococcus* populations in a stratified water column in the Eastern North Atlantic Ocean. *Appl. Environ. Microbiol.* **65**, 2585–2591 (1999).

12. Rocap, G., Distel, D. L., Waterbury, J. B. & Chisholm, S. W. Resolution of *Prochlorococcus* and *Synechococcus* ecotypes by using 16S-23S ribosomal DNA internal transcribed spacer sequences. Appl. Environ. Microbiol. **68**, 1180–1191 (2002).

13. Zwirglmaier, K., Jardillier, L., Ostrowski, M., Mazard, S., Garczarek, L., Vaulot, D., Not, F., Massana, R., Ulloa, O. & Scanlan, D.J., 2008. Global phylogeography of marine *Synechococcus* and *Prochlorococcus* reveals a distinct partitioning of lineages among oceanic biomes. *Environ. Microbiol.* **10**, 147-161 (2008).

14. Martiny, A. C., Tai, A. P. K., Veneziano, D., Primeau, F. & Chisholm, S. W. Taxonomic resolution, ecotypes and the biogeography of *Prochlorococcus*. *Environ*. *Microbiol*. **11**, 823–832 (2009).

15. Malmstrom, R.R., Coe, A., Kettler, G.C., Martiny, A.C., Frias-Lopez, J., Zinser, E.R. & Chisholm, S.W. Temporal dynamics of *Prochlorococcus* ecotypes in the Atlantic and Pacific oceans. *The ISME J.* **4**, 1252 (2010).

16. Biller, S.J., Berube, P.M., Lindell, D. & Chisholm, S.W. *Prochlorococcus*: the structure and function of collective diversity. *Nature Rev. Microbiol.* **13** 13 (2015).

17. Moore, L. R., & S. W. Chisholm. Photophysiology of the marine cyanobacterium *Prochlorococcus*: ecotypic differences among cultured isolates. *Limnol. Oceanogr.* **44**, 628-638 (1999).

18. J.T.O. Kirk The nature of the underwater light field Light and Photosynthesis *In* Aquatic Ecosystems, Cambridge University Press (1994)

19. B.P. Palenik & R. Haselkorn. Multiple evolutionary origins of prochlorophytes, the chlorophyll *b*-containing prokaryotes. *Nature* **355**, 265-267 (1992).

20. Urbach, E., Robertson, D.L. & Chisholm, S. W. Multiple evolutionary origins of prochlorophytes within the cyanobacterial radiation. *Nature* **355**, 267 (1992).

21. Scanlan, D.J. & West, N.J. Molecular ecology of the marine cyanobacterial genera *Prochlorococcus* and *Synechococcus*. *FEMS Microbiol. Ecol.* **40** 1-12 (2002).

22. Ting, C.S., Rocap, G., King, J. & Chisholm, S.W. Cyanobacterial photosynthesis in the oceans: the origins and significance of divergent light-harvesting strategies. *Trends Microbiol*. **10**, 134-142 (2002)

23. La Roche, J., Van der Staay, G.W.M., Partensky, F., Ducret, A., Aebersold, R., Li, R., Golden, S.S., Hiller, R.G., Wrench, P.M., Larkum, A.W.D. & Green, B.R. Independent evolution of the prochlorophyte and green plant chlorophyll a/b light-harvesting proteins. *Proc. Natl Acad. Sci* USA, **93** 15244-15248 (1996).

24. Chen, M. & Bibby, T. S. Photosynthetic apparatus of antenna-reaction centres supercomplexes in oxyphotobacteria: insight through significance of Pcb/IsiA proteins. *Photosynthesis Res.* **86** 165-173 (2005).

25. Bibby, T.S., Nield, J., Partensky, F. & Barber, J. Oxyphotobacteria: Antenna ring around photosystem I. *Nature*, **413** 590 (2001a).

26. Bibby, T.S., Mary, I., Nield, J., Partensky, F. & Barber, J. Low-light-adapted *Prochlorococcus* species possess specific antennae for each photosystem. *Nature*, **424** 1051 (2003).

27. Bibby, T.S., Nield, J. & Barber, J. Iron deficiency induces the formation of an antenna ring around trimeric photosystem I in cyanobacteria. *Nature*, **412** 743. (2001b).

28. Boekema, E.J., Hifney, A., Yakushevska, A.E., Piotrowski, M., Keegstra, W., Berry, S., Michel, K.P., Pistorius, E.K. & Kruip, J. A giant chlorophyll–protein complex induced by iron deficiency in cyanobacteria. *Nature*, **412** 745 (2001).

29. Ting, C.S., Hsieh, C., Sundararaman, S., Mannella, C. & Marko, M. Cryo-electron tomography reveals the comparative three-dimensional architecture of *Prochlorococcus*, a globally important marine cyanobacterium. *J. Bacteriol.* **189** 4485-4493 (2007)

30. Kirchhoff, H., Lenhert, S., Büchel, C., Chi, L. & Nield, J. Probing the organization of photosystem II in photosynthetic membranes by atomic force microscopy. *Biochemistry* **47** 431–440 (2008).

31. Sznee, K., Dekker, J.P., Dame, R.T., van Roon, H., Wuite, G.J.L. & Frese, R.N. Jumping mode atomic force microscopy on grana membranes from spinach. *J. Biol. Chem.* **286** 39164–39171 (2011).

32. Johnson, M.P., Vasilev, C., Olsen, J.D. & Hunter, C.N. Nanodomains of cytochrome b_6f and photosystem II complexes in spinach grana thylakoid membranes. *Plant Cell* **26** 3051–3061 (2014).

33. Onoa, B., Schneider, A.R., Brooks, M.D., Grob, P., Nogales, E., Geissler, P.L., Niyogi, K.K. & Bustamante, C. Atomic force microscopy of photosystem II and its unit cell clustering quantitatively delineate the mesoscale variability in *Arabidopsis* thylakoids. *PloS One*, **9**, p.e101470 (2014)

34. Phuthong, W., Huang, Z., Wittkopp, T.M., Sznee, K., Heinnickel, M.L., Dekker, J.P., Frese, R.N., Prinz, F.B. & Grossman, A.R. The use of contact mode atomic force microscopy in aqueous medium for structural analysis of spinach photosynthetic complexes. *Plant Physiol.* **169** 1318–1332 (2015).

35. Tietz, S., Puthiyaveetil, S., Enlow, H.M., Yarbrough, R., Wood, M., Semchonok, D.A., Lowry, T., Li, Z., Jahns, P., Boekema, E.J. & Lenhert, S. Functional implications of photosystem II crystal formation in photosynthetic membranes. *J. Biol. Chem.* **290** 14091-14106 (2015).

36. Wood, W.H., MacGregor-Chatwin, C., Barnett, S.F., Mayneord, G.E., Huang, X., Hobbs, J.K., Hunter, C.N. & Johnson, M.P. Dynamic thylakoid stacking regulates the balance between linear and cyclic photosynthetic electron transfer. *Nature Plants*, **4** 116 (2018)

37. Liu, L.N. & Scheuring, S. Investigation of photosynthetic membrane structure using atomic force microscopy. *Trends in Plant Science* **18** 277-286 (2013).

38. Kumar, S., Cartron, M.L., Mullin, N., Qian, P., Leggett, G.L., Hunter, C.N., & Hobbs, J.K. Direct imaging of protein organisation in an intact bacterial organelle using high-resolution Atomic Force Microscopy. *ACS Nano* **11** 126-133 (2017).

39. MacGregor-Chatwin, C., Sener, M., Barnett, S.F., Hitchcock, A., Barnhart-Dailey, M.C., Maghlaoui, K., Barber, J., Timlin, J.A., Schulten, K. & Hunter, C.N. Lateral segregation of photosystem I in cyanobacterial thylakoids. *The Plant Cell*, **29** 1119-1136 (2017).

40. Casella, S., Huang, F., Mason, D., Zhao, G.Y., Johnson, G.N., Mullineaux, C.W. & Liu, L.N. Dissecting the native architecture and dynamics of cyanobacterial photosynthetic machinery. *Molecular Plant*, **10** 1434-1448 (2017).

41. Jordan, P., Fromme, P., Witt, H.T., Klukas, O., Saenger, W. & Krauß, N. Three-dimensional structure of cyanobacterial photosystem I at 2.5 Å resolution. *Nature*, **411** 909 (2001).

42. Malavath, T., Caspy, I., Netzer-El, S.Y., Klaiman, D. & Nelson, N. Structure and function of wild-type and subunit-depleted photosystem I in Synechocystis. *Biochimica et Biophysica Acta (BBA)-Bioenergetics*, **1859** 645-654 (2018).

43. Kubota-Kawai, H., Mutoh, R., Shinmura, K., Sétif, P., Nowaczyk, M.M., Rögner, M., Ikegami, T., Tanaka, H. and Kurisu, G., 2018. X-ray structure of an asymmetrical trimeric ferredoxin–photosystem I complex. *Nature plants*, **4** 218-224 (2018).

44. Umena, Y., Kawakami, K., Shen, J.R. & Kamiya, N. Crystal structure of oxygen-evolving photosystem II at a resolution of 1.9 Å. *Nature*, **473** 55 (2011).

45. Jeffrey, S.T. & Humphrey, G.F. New spectrophotometric equations for determining chlorophylls a, b, c1 and c2 in higher plants, algae and natural phytoplankton. *Biochemie und Physiologie der Pflanzen*, **167** 191-194 (1975).

46. Rippka, R., Coursin, T., Hess, W., Lichtlé, C., Scanlan, D.J., Palinska, K.A., Iteman, I., Partensky, F., Houmard, J. & Herdman, M. Prochlorococcus marinus Chisholm et al. 1992 subsp. pastoris subsp. nov. strain PCC 9511, the first axenic chlorophyll a2/b2-containing cyanobacterium (Oxyphotobacteria). *International Journal of Systematic and Evolutionary Microbiology*, **50** 1833-1847 (2000).

47. Nečas, D. & Klapetek, P. Gwyddion: an open-source software for SPM data analysis. *Open Physics*, **10** 181-188 (2012).

48. Wolfram Research, Inc., Mathematica, Version 11.3, Champaign, IL (2018).

49. Humphrey, W.; Dalke, A.; Schulten, K. VMD − Visual Molecular Dynamics. *J. Mol. Graphics*, **14**, 33−38 (1996).

50. Sener, M.K., Park, S., Lu, D., Damjanović, A., Ritz, T., Fromme, P & Schulten, K. Excitation migration in trimeric cyanobacterial photosystem I. *J. Chem. Phys.* **120**: 11183–11195 (2004).

51. Hitchcock A, Jackson P.J., Chidgey J.W., Dickman M.J., Hunter C.N. and Canniffe D.P. Biosynthesis of chlorophyll a in a purple bacterial phototroph and assembly into a plant chlorophyll-protein complex *ACS Synth. Biol.* **5** 948-954 (2016).

920 52. Cox, J. and Mann, M. MaxQuant enables high peptide identification rates, individualized
921 p.p.b.-range mass accuracies and proteome-wide protein quantification. *Nat Biotechnol.* **26**
922 1367-1372 (2008).

923

924 53. Schwanhäusser, B., Busse, D., Li, N., Dittmar, G., Schuchhardt, J., Wolf, J., Chen, W. & Selbach,
925 M. Global quantification of mammalian gene expression control. *Nature* **473** 337-342 (2011).

926

927 54. Fabre, B., Lambour, T., Bouyssié, D., Menneteau, T., Monsarrat, B., Burlet-Schiltz, O. &
928 Bousquet-Dubouch, M.-P. Comparison of label-free quantification methods for the
929 determination of protein complexes subunits stoichiometry. *EuPA Open Proteomics* **4** 82-86
930 (2014).

931

932 55. Tyanova, S., Temu, T., Sinitcyn, P., Carlson, A., Hein, M., Geiger, T., Mann, M. & Cox, J. The
933 Perseus computational platform for comprehensive analysis of (prote) omics data. *Nature*
934 *Methods*, **13**, 731-740 (2016).

935

936 56. García-Plazaola, J.I. & Becerril, J.M. A rapid high-performance liquid chromatography method
937 to measure lipophilic antioxidants in stressed plants: simultaneous determination of
938 carotenoids and tocopherols. *Phytochemical Analysis*, **10** 307-313 (1999).

939

940 57. Kalb Jr, V.F. & Bernlohr, R.W. A new spectrophotometric assay for protein in cell extracts.
941 *Analytical biochemistry*, **82** 362-371 (1977).